Dynamics of a Multimode System Coupled to Multiple Heat Baths Probed by Two-Dimensional Infrared Spectroscopy†

Akihito Ishizaki* and Yoshitaka Tanimura

Department of Chemistry, Graduate School of Science, Kyoto University, Kyoto 606-8502, Japan

Received: April 13, 2007; In Final Form: July 22, 2007

Reduced equation of motion for a multimode system coupled to multiple heat baths is constructed by extending the quantum Fokker−Planck equation with low-temperature correction terms (*J. Phys. Soc. Jpn.* **2005**, *74*, 3131). Unlike such common approaches used to describe intramolecular multimode vibration as a Bloch−Redfield theory and a stochastic theory, the present formalism is defined by the molecular coordinates. To explore the correlation among different modes through baths, we consider two cases of system−bath couplings. One is a correlated case in which two modes are coupled to a single bath, and the other is an uncorrelated case in which each mode is coupled to a different bath. We further classify the correlated case into two cases, the plus- and minus-correlated cases, according to distinct correlation manners. For these, one-dimensional and two-dimensional infrared (2D-IR) spectra are calculated numerically by solving the equation of motion. It is demonstrated that 2D-IR spectroscopy has the ability to analyze the correlation of fluctuation−dissipation processes among different modes.

1. Introduction

Vibrational spectroscopy has provided important insight into the structural and dynamic properties of chemical and biophysical systems in condensed phases. However, most of the conventional one-dimensional (1D) vibrational spectroscopies, which project the nuclear motion onto a single frequency or time axis, cannot extract the wealth of information unambiguously. This is because we cannot separate a variety of dynamic contributions to the vibrational line shapes on the 1D axis. To disentangle the 1D line shapes, one needs to explore multidimensional observables, which project the microscopic dynamics onto more than two axes.

Over the past decade, extensive theoretical, computational, and experimental efforts have been made for multidimensional vibrational spectroscopy[1−8] to have a variety of information on molecules in condensed phases. Consequently, the multidimensional spectroscopy has been proven to be valuable and versatile tools for diverse topics in condensed-phase chemical dynamics. Especially, objects under study in two-dimensional infrared (2D-IR) spectroscopy have definitely spread very wide: structures and dynamics of peptides,[9−15] conformational changes in protein,[16−18] water dynamics,[19] hydrogen-bond dynamics,[20−25] solute−solvent interactions,[26,27] quantum tunneling processes,[28−30] and fast chemical exchange in molecular complexes.[31−33]

Multidimensional vibrational spectroscopy is the optical counterpart of multidimensional NMR such as COSY and NOESY, which are powerful tools for organic structural analysis and structural biology.[34] In 2D-NMR and 2D-IR experiments, the data sets are represented in the 2D frequency space. The 2D frequency space allows us to separate the dynamic contributions from various Liouville pathways. We can, therefore, identify coupled modes visually from the off-diagonal peaks.[35−40] Furthermore, because the 2D line shapes are very sensitive to a time-evolution of the environment, we can estimate the characteristic timescales of environment.[41]

On another front, the vibrational dynamics in 2D-IR spectroscopy are very complicated compared to the spin dynamics in 2D-NMR. Unlike spin dynamics, vibrational dynamics cannot be generally described within the conventional frameworks of quantum master equations. The well-known Redfield theory[42] cannot always be applied to such a low-temperature system as intramolecular vibration, where quantum effects play a major role. The physically valid density operators should have positive (or non-negative) eigenvalues because the eigenvalues correspond to state probabilities. In a low-temperature case, however, a time evolution described by the Redfield equation does not necessarily conserve the positivity property. This difficulty is called *the positivity problem*. As a way to ensure the property, one performs the secular approximation, which involves averaging over the rapidly oscillating terms in the equation and is known as the rotating-wave approximation. However, the approximation has no guarantee of maintaining the original dynamic properties.[43] In addition, the equation employs the perturbative manner for the system−bath interaction and the Markov approximation. Hence, it cannot handle strong system−bath couplings and memory effects.

As was shown by Tanimura et al., such systems can be treated by utilizing a tridiagonal hierarchy of equations.[44−50] For a low-temperature case, the structure of hierarchy becomes very complicated because of the quantum nature of the heat bath characterized by Matsubara frequencies.[51] Then, Ishizaki and Tanimura clarified the structure of hierarchy and found a rigorous and simple way to terminate the hierarchy, reducing the quantum Fokker−Planck equation with low-temperature correction terms (QFP-LTC).[52] Along the line of hierarchy formalism, different formulations have been tested,[53−56] but practical problems demonstrated so far, such as vibrational dephasing problems of 2D-IR spectroscopy, were only from the QFP-LTC approach.[57] Here, we extend previous analysis of a

† Part of the "Sheng Hsien Lin Festschrift".

* Corresponding author. E-mail address: ishizaki@kuchem.kyoto-u.ac.jp.

10.1021/jp072880a CCC: $37.00
Published on Web 09/20/2007

single-mode system to multimode systems coupled to multiple baths by further extending the QFP-LTC formalism. Special attention will be paid to explore the correlation of fluctuation−dissipation processes among different modes by means of the 2D-IR spectroscopy. This work is motivated by the experiment performed by Demirdöven, Khalil, and Tokmakoff.[6,58] They reported on the 2D-IR experiment of the correlation effects in the solvation dynamics of coupled vibrational modes. As a model system to probe the correlated dynamics, they studied the coupled symmetric and asymmetric carbonyl [−C≡O] stretching modes of dicarbonyl acetylacetonato rhodium(I) [Rh-$(CO)_2C_5H_7O_2$] dissolved in chloroform. Their analyses were based on a quasi-static energy-level model assuming a complete separation of the extremely fast (homogeneous limit) and extremely slow (inhomogeneous limit) components. In this paper, we employ more general model expressed in molecular coordinates and apply rigorous dynamical theory for arbitrary time-scale components of the system and baths. Although 2D-IR experiments are carried out at room temperature, we need to include the low-temperature correction terms. This is because, in the intramolecular vibrational motion under discussion, the temperature is much lower than the vibrational excitation energy, where quantum effects play a dominant role.

This paper is organized as follows: In Section 2, we introduce the quantum dissipative equation, which can describe the dynamics of the multimode system coupled to multiple heat baths. In Section 3, numerical results for nonlinear optical signals including 2D-IR spectra are presented and discussed. Section 4 is devoted to concluding remarks.

2. Multimode System Coupled to Multiple Baths: Reduced Equation of Motion

We consider a multimode system described by dimensionless coordinates, $\boldsymbol{q} \equiv (q_1, q_2, \ldots)$, and their conjugate momenta, $\boldsymbol{p} \equiv (p_1, p_2, \ldots)$. The Hamiltonian is given by

$$\hat{H} = \sum_s \frac{\hbar\omega_s}{2}\hat{p}_s^2 + U(\hat{\boldsymbol{q}}) \tag{2.1}$$

where $U(\boldsymbol{q})$ is the molecular potential for the vibrational motion and is separated into harmonic parts and an anharmonic part as follows:

$$U(\boldsymbol{q}) = \sum_s \frac{\hbar\omega_s}{2} q_s^2 + U_{\mathrm{anh}}(\boldsymbol{q}) \tag{2.2}$$

For the potential, we define the characteristic frequency as $\omega_c \equiv \max_s(\omega_s)$.

To model an intramolecular vibrational motion in a condensed phase, we consider the system coupled to multiple heat baths each of which consists of harmonic oscillators. The total Hamiltonian is expressed as

$$\hat{H}_{\mathrm{tot}} = \hat{H} + \sum_\alpha [\hat{H}_{\mathrm{bath}}^{(\alpha)} + \hat{H}_{\mathrm{int}}^{(\alpha)}] \tag{2.3}$$

Here, the bath and system−bath interaction Hamiltonians are expressed as

$$\hat{H}_{\mathrm{bath}}^{(\alpha)} + \hat{H}_{\mathrm{int}}^{(\alpha)} = \sum_j \left[\frac{\hat{\pi}_{\alpha j}^2}{2} + \frac{\omega_{\alpha j}^2}{2}\left(\hat{\xi}_{\alpha j} - \frac{c_{\alpha j}}{\omega_{\alpha j}^2}W_\alpha(\hat{\boldsymbol{q}})\right)^2\right] \tag{2.4}$$

where the parameters $\xi_{\alpha j}$, $\pi_{\alpha j}$, and $\omega_{\alpha j}$ are the mass-weighted coordinate, conjugate momentum, and frequency of the jth oscillator in the αth bath, respectively. In eq 2.4, the interaction between the multimode system and the αth bath is expressed as $H_{\mathrm{int}}^{(\alpha)}(\boldsymbol{q}, \{\xi_{\alpha j}\}) = -W_\alpha(\boldsymbol{q})\sum_j c_{\alpha j}\xi_{\alpha j}$, where $W_\alpha(\boldsymbol{q})$ is a function whose dimension is the same as $\boldsymbol{q}$. We have included the counter term $\Delta U_\alpha(\boldsymbol{q}) \equiv W_\alpha(\boldsymbol{q})^2\sum_j c_{\alpha j}^2/2\omega_{\alpha j}^2$ to maintain the translational symmetry of the Hamiltonian for $U(\boldsymbol{q}) = 0$.[49]

The key quantity of interest is the reduced density operator, $\hat{\rho}(t) \equiv \mathrm{Tr}_{\mathrm{baths}}\{\hat{\rho}_{\mathrm{tot}}(t)\}$, that is, the partial trace of the total density operator over the optically inactive bath degrees of freedom $\{\xi_\alpha j\}$. Here, we suppose that the total system at the initial time $t = t_i$ is in *the uncorrelated product state* of the form $\hat{\rho}_{\mathrm{tot}}(t_i) \propto \hat{\rho}(t_i)\prod_\alpha \exp(-\beta_\alpha\hat{H}_{\mathrm{bath}}^{(\alpha)})$. Then, the reduced density operator evolves in times as follows

$$\hat{\rho}(t) = \hat{\mathscr{G}}(t; t_i)\hat{\rho}(t_i) \tag{2.5}$$

where the matrix element of the Liouville space propagator $\hat{\mathscr{G}}(t; t_i)$ can be expressed in the path integral form as

$$\mathscr{G}(\boldsymbol{q}, \boldsymbol{q}', t; \boldsymbol{q}_i, \boldsymbol{q}_i', t_i) = \int_{(\boldsymbol{q}_i,t_i)}^{(\boldsymbol{q},t)} \mathscr{D}\boldsymbol{q}\int_{(\boldsymbol{q}_i',t_i)}^{(\boldsymbol{q}',t)} \mathscr{D}\boldsymbol{q}' e^{iS^{\mathrm{eff}}[\boldsymbol{q}]/\hbar}\left[\prod_\alpha \mathscr{F}_\alpha[\boldsymbol{q}, \boldsymbol{q}']\right] e^{-iS^{\mathrm{eff}}[\boldsymbol{q}']/\hbar} \tag{2.6}$$

Here, $S^{\mathrm{eff}}[\boldsymbol{q}]$ is the action corresponding to the renormalized system Hamiltonian, $H^{\mathrm{eff}} \equiv H + \sum_\alpha \Delta U_\alpha(\boldsymbol{q})$, and $\mathscr{F}_\alpha[\boldsymbol{q}, \boldsymbol{q}']$ is the Feynman−Vernon influence functional[59] for the αth bath whose character is specified by the spectral density, $I_\alpha(\omega) \equiv \pi\sum_j[c_{\alpha j}^2/2\omega_{\alpha j}]\delta(\omega - \omega_{\alpha j})$. In this paper, we take an Ohmic spectral density with the Lorentz−Drude regularization:

$$I_\alpha(\omega) = \frac{\hbar\zeta_\alpha}{\omega_c}\omega\frac{\gamma_\alpha^2}{\omega^2 + \gamma_\alpha^2} \tag{2.7}$$

The parameters γ_α and ζ_α are related to the correlation time and the strength of noise by the αth bath, respectively. This can be seen from the symmetrized correlation function of the αth bath collective coordinate $\hat{X}_\alpha(t) \equiv \sum_j c_{\alpha j}\hat{x}_{\alpha j}(t)$:

$$\frac{1}{2}\langle\{\hat{X}_\alpha(t), \hat{X}_\alpha(0)\}\rangle_{\mathrm{B}} \propto \frac{\zeta_\alpha}{\beta_\alpha}\gamma_\alpha e^{-\gamma_\alpha t} + \Lambda_\alpha(t) \tag{2.8}$$

with

$$\Lambda_\alpha(t) \equiv -\frac{\zeta_\alpha}{\beta_\alpha}\sum_{k=1}^{\infty}\frac{2\gamma_\alpha^2}{\nu_{\alpha k}^2 - \gamma_\alpha^2}(\gamma_\alpha e^{-\gamma_\alpha t} - \nu_{\alpha k}e^{-\nu_{\alpha k}t}) \tag{2.9}$$

where $\{\ ,\ \}$ stands for the anticommutator, and $\langle\cdots\rangle_{\mathrm{B}}$ is the thermal average with respect to the bath degrees of freedom. Equation 2.9 involving the bosonic Matsubara frequency $\nu_{\alpha k} = 2\pi k/\beta_\alpha\hbar$ ($k \geq 1$) represents a quantum effect of the αth bath noise. In the high-temperature region $\beta_\alpha\hbar\gamma_\alpha/2 \ll 1$, the contribution of $\Lambda_\alpha(t)$ to eq 2.8 becomes vanishingly small. Therefore, eq 2.8 indicates that the bath oscillators disturb the system with the colored noise, which has an exponential time correlation. However, just because the contribution of eq 2.9 is vanishingly small does not mean that we can disregard it. The disregard of this term at low temperatures characterized by $\beta_\alpha\hbar\omega_c/2 \gtrsim 1$ destroys the quantum interference between the system and the bath and then gives rise to such an unphysical result as *the positivity problem*, where the populations of the excited states become negative. For the wholesome description

of quantum dissipative dynamics, it is indispensable to construct the equations involving the effects of eq 2.9. In a similar manner described in refs 52 and 57, we can construct the hierarchy of equations for a system coupled to multiple heat baths. Here, we can obtain the dynamic equation for the reduced density operator eq 2.5 as follows:

$$\frac{\partial}{\partial t}\hat{\rho}(\boldsymbol{J};t) = -i\hat{\mathscr{L}}^{\mathrm{eff}}\hat{\rho}(\boldsymbol{J};t) - \sum_{\alpha}\left[\sum_{k=0}^{K_\alpha} j_{\alpha k}\nu_{\alpha k} + \hat{\Xi}_\alpha\right]\hat{\rho}(\boldsymbol{J};t) - \sum_{\alpha}\sum_{k=0}^{K_\alpha}\hat{\Phi}_\alpha\hat{\rho}(\boldsymbol{J}_{\alpha k+};t) - \sum_{\alpha}\sum_{k=0}^{K_\alpha} j_{\alpha k}\nu_{\alpha k}\hat{\Theta}_{\alpha k}\hat{\rho}(\boldsymbol{J}_{\alpha k-};t) \quad (2.10)$$

where we introduce the set of hierarchy elements $\boldsymbol{J} \equiv \{\boldsymbol{j}_1, \boldsymbol{j}_2, \ldots\}$ with the $K_\alpha + 1$-dimensional vector for αth bath defined by $K_\alpha + 1$ non-negative integers, $\boldsymbol{j}_\alpha \equiv (j_{\alpha 0}, j_{\alpha 1}, \ldots, j_{\alpha K_\alpha})$. We defined $\nu_{\alpha 0} \equiv \gamma_\alpha$ and introduced the notation $\boldsymbol{J}_{\alpha k\pm} = \{\boldsymbol{j}_1, \ldots, \boldsymbol{j}_{\alpha k\pm}, \ldots\}$ with $\boldsymbol{j}_{\alpha k\pm} \equiv (j_{\alpha 0}, \ldots, j_{\alpha k} \pm 1, \ldots, j_{\alpha K_\alpha})$. The value of K_α is determined so as to satisfy[52]

$$\nu_{\alpha K} \gg \omega_c \quad (2.11)$$

Note that only $\hat{\rho}(\boldsymbol{J} = \boldsymbol{0}; t) = \hat{\rho}(t)$ describes the dynamics to be measured, whereas the other elements $\hat{\rho}(\boldsymbol{J} \neq \boldsymbol{0}; t)$ are the auxiliary operators being introduced in order to take into account a correlation between the system and the bath as the memory effect and the quantum interference. In eq 2.10, $i\hat{\mathscr{L}}^{\mathrm{eff}} \equiv (i/\hbar)\times[\hat{H} + \sum_\alpha \Delta U_\alpha(\hat{\boldsymbol{q}})]^\times$ is the quantal Liouvillian of the system, where the counter term $\Delta U_\alpha(\hat{\boldsymbol{q}})$ is expressed as

$$\Delta U_\alpha(\hat{\boldsymbol{q}}) = \hbar\frac{\zeta_\alpha\gamma_\alpha}{2\omega_c}W_\alpha(\hat{\boldsymbol{q}})^2 \quad (2.12)$$

$\hat{\Phi}_\alpha$, $\hat{\Theta}_{\alpha k}$, and $\hat{\Xi}_\alpha$ are the αth bath-induced relaxation operators defined by and

$$\hat{\Phi}_\alpha \equiv iW_\alpha(\hat{\boldsymbol{q}})^\times \quad (2.13a)$$

$$\hat{\Theta}_{\alpha 0} \equiv i\frac{\zeta_\alpha}{\beta_\alpha\hbar\omega_c}[z_\alpha\cot z_\alpha\, W_\alpha(\hat{\boldsymbol{q}})^\times - iz_\alpha W_\alpha(\hat{\boldsymbol{q}})^\circ] \quad (2.13b)$$

$$\hat{\Theta}_{\alpha k} \equiv i\frac{\zeta_\alpha}{\beta_\alpha\hbar\omega_c}\frac{2z_\alpha^2}{\pi^2k^2 - z_\alpha^2}W_\alpha(\hat{\boldsymbol{q}})^\times \quad (k \geq 1) \quad (2.13c)$$

$$\hat{\Xi}_\alpha \equiv \sum_{k=1}^{K_\alpha}\hat{\Phi}_\alpha\hat{\Theta}_{\alpha k} + \frac{\zeta_\alpha}{\beta_\alpha\hbar\omega_c}(1 - z_\alpha\cot z_\alpha)[W_\alpha(\hat{\boldsymbol{q}})^\times]^2 \quad (2.13d)$$

with $z_\alpha \equiv \beta_\alpha\hbar\gamma_\alpha/2$. In the above, we have introduced the hyperoperator notations

$$\hat{\mathscr{O}}^\times\hat{f} \equiv \hat{\mathscr{O}}\hat{f} - \hat{f}\hat{\mathscr{O}}, \qquad \hat{\mathscr{O}}^\circ\hat{f} \equiv \hat{\mathscr{O}}\hat{f} + \hat{f}\hat{\mathscr{O}} \quad (2.14)$$

for any operator $\hat{\mathscr{O}}$ and operand operator $\hat{f}$.

The multidimensional hierarchy equations, eq 2.10, continue to infinity, which is not easy to solve numerically. To terminate eq 2.10 at the finite stages, we introduce the following terminator[52,57]

$$\frac{\partial}{\partial t}\hat{\rho}(\boldsymbol{J};t) \simeq -i\hat{\mathscr{L}}^{\mathrm{eff}}\hat{\rho}(\boldsymbol{J};t) - \sum_\alpha\hat{\Xi}_\alpha\hat{\rho}(\boldsymbol{J};t) \quad (2.15)$$

which is valid for the integers $j_{\alpha 0}, j_{\alpha 1}, \ldots, j_{\alpha K}$ satisfying

$$N_\alpha \equiv \sum_{k=0}^{K_\alpha} j_k \gg \frac{\omega_c}{\max(\gamma_\alpha, \nu_{\alpha 1})} \quad (2.16)$$

In practice, as demonstrated in ref 52, we may use the lower values of K_α and N_α, which do not satisfy eqs 2.11 and 2.16, respectively. Equation 2.10 with eq 2.15 has applicability to a low-temperature system strongly coupled to the heat bath without employing the rotating-wave approximation for the system−bath interaction; eq 2.10 with eq 2.15 is free from the positivity problem. This advantage deserves explicit emphasis.

3. Dynamics of the Multimode System Probed by 2D-IR Spectra

In this section, we present the vibrational spectra calculated for an optically active two-mode system

$$\hat{H} = \frac{\hbar\omega_1}{2}\hat{p}_1^2 + \frac{\hbar\omega_2}{2}\hat{p}_2^2 + U(\hat{q}_1, \hat{q}_2) \quad (3.1)$$

under various system−bath interactions. Here, we consider the nonlinearly coupled Morse oscillators system whose potential is given by

$$U(q_1, q_2) = \sum_{s=1}^{2}U_s(q_s) + \hbar\left(\frac{g_{112}}{2}q_1^2q_2 + \frac{g_{122}}{2}q_1q_2^2\right) \quad (3.2)$$

where

$$U_s(q_s) = \frac{\hbar\omega_s}{2a_s^2}[1 - \exp(-a_sq_s)]^2 \quad (3.3)$$

We describe the system in terms of the energy eigenstates of each vibrational mode in the case of $g_{112} = g_{122} = 0$, $\{|v_1, v_2\rangle\} \equiv \{|v_1\rangle \otimes |v_2\rangle\}$, where $|v_s\rangle$ is the eigenstate belonging to the vth eigenvalues $E_{s,v}$ of the sth mode. The two-mode system is specified by the parameters

$$\omega_1 = 1565.65\ \mathrm{cm}^{-1}, \qquad \omega_2 = 1666.66\ \mathrm{cm}^{-1} \quad (3.4)$$

$$a_1 = a_2 = 0.1 \quad (3.5)$$

$$g_{112} = g_{122} = -40\ \mathrm{cm}^{-1} \quad (3.6)$$

and $\omega_c = \max(\omega_1, \omega_2) = \omega_1$. In addition, we assume the dipole moment to be the following form

$$\mu(\hat{\boldsymbol{q}}) = \mu_1q_1 + \mu_2q_2 \quad (3.7)$$

and we set $\mu_1 = \mu_2 = 1$ to calculate the optical signals.

We begin with the two-mode system coupled to a single heat bath: the case of only $\alpha = 1$. For simplicity of the later discussion, the system−bath interaction $H_{\mathrm{int}}^{(1)}(\boldsymbol{q},\{\xi_{1j}\})$ in eq 2.4 is assumed to be of the form

$$W_1(\boldsymbol{q})\sum_j c_{1j}\xi_{1j} = \left(\frac{V_{11}}{2}q_1^2 + \frac{V_{22}}{2}q_2^2\right)\sum_j c_{1j}\xi_{1j} \quad (3.8)$$

This interaction induces not only the dissipation but also the curvature fluctuation of the potential surface $U(q_1, q_2)$ in accordance with the time evolution of the bath coordinates $\{\xi_{1j}\}$.[46−49] Furthermore, we consider the two sets of the value

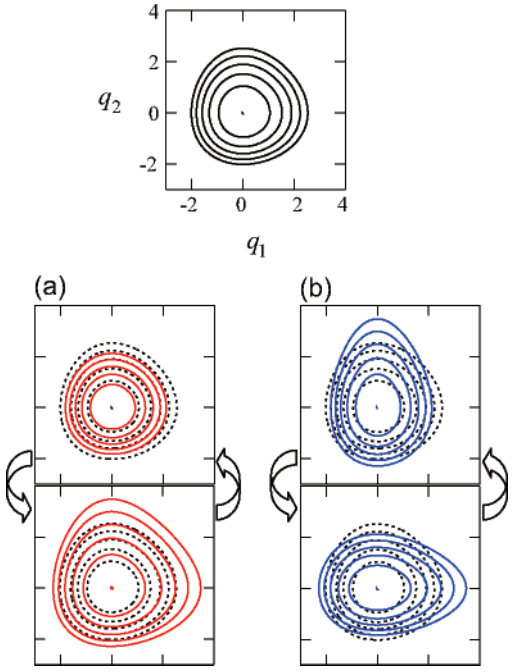

Figure 1. Schematic illustration of correlated fluctuations of the potential energy surface of the two-mode system. The top panel shows the contour lines of the unperturbed surface as the function of two molecular coordinates. In panel a, the red lines represent the perturbed contour lines by the + correlated fluctuation. In panel b, the blue lines represent the contour lines modulated by the − correlated fluctuation. In a and b, the black dashed lines are the unperturbed contours, and the arrows denote that the potential energy surface fluctuates around the unperturbed state. The + correlated and − correlated fluctuations deform the potential surface in distinct manners.

for V_{ss}: (a) $(V_{11}, V_{22}) = (+1, +1)$ and (b) $(V_{11}, V_{22}) = (+1, -1)$. As we show in the schematic illustration in Figure 1, the bath modulates the system in distinct manner. In case (a), the bath modulates the curvature along the q_1 axis and that along the q_2 axis in the same direction, whereas in case (b), the bath modulates the curvatures along two axes in opposite directions. We call the fluctuations in (a) and (b) + *correlated fluctuation* and − *correlated fluctuation*, respectively. For both (a) and (b), the system−bath coupling parameters are set to be $\gamma_1 = 0.004\omega_c$ and $\zeta_1 = 0.4\omega_c$. The temperature of the heat bath is $T = 300$ K. From these parameters, the amplitude of the frequency fluctuation in the sth mode ($s = 1, 2$) can be estimated at $\Delta_s = 0.0075\omega_c$. (See eq 3.18 in ref 57.) Then, we have $\Delta_s/\gamma_1 = 1.87$. This value is in the so-called spectral diffusion regime with moderate inhomogeneity. Note that the extreme cases, $\Delta_s/\gamma_1 \ll 1$ and $\Delta_s/\gamma_1 \gg 1$ are called the homogeneous and inhomogeneous limit, respectively.

As the third case (c), we consider the two-mode system where the sth mode ($s = 1, 2$) is coupled to the sth heat bath. The sth system−bath interaction is assumed to be in the form

$$W_s(\boldsymbol{q}) \sum_j c_{sj}\xi_{sj} = \frac{V_{ss}}{2} q_s^2 \sum_j c_{sj}\xi_{sj} \tag{3.9}$$

Because the baths do not interact with each other, the fluctuations along the two axes in the potential surface do not correlate. Therefore, we call this case *uncorrelated fluctuation*. For this case, the system−bath parameters are set to be $\gamma_1 = \gamma_2 = 0.004\omega_c$ and $\zeta_1 = \zeta_2 = 0.4\omega_c$. The temperatures of the two baths are assumed to be the same as that in the single bath case, $T = 300$ K.

To obtain signals, we numerically integrate eq 2.10 with eq 2.15 by using the fourth-order Runge−Kutta method. The time step for the finite difference expression for $\partial\hat{\rho}(\boldsymbol{J}, t)/\partial t$ is $\delta t = (1/\omega_c) \times 0.01$. The system is represented by the lowest four energy eigenstates of the respective vibrational modes in order to carry out the calculations. We choose the hierarchy and the number of the Matsubara frequencies $N_\alpha = 7-15$ and $K_\alpha = 1-4$, respectively. As was mentioned in Section 1, by the virtue of the low-temperature correction terms, the present equations of motion maintain the positivity property, where most of the reduced equation of motion could not be certified. The accuracy of the numerical calculations is checked by changing the number of the energy eigenstates and the values of δt, N_α, and K_α.

For resonant third-order nonlinear spectroscopic experiments, we apply the three short pulses, tuned to the molecular vibration of interest, with wave vectors $\boldsymbol{k}_a$, $\boldsymbol{k}_b$, and $\boldsymbol{k}_c$ at time $t = t_a$, t_b, and t_c, respectively. These pulses generate the four-wave-mixing signal field in the phase-matched directions. In this paper, we consider the signals generated in the phase-matched direction $\boldsymbol{k}_S = \boldsymbol{k}_c + \boldsymbol{k}_b - \boldsymbol{k}_a$. The signal detected at time t is described by a nonlinear response function, which depends on three time intervals referred to as the evolution period τ_1, the waiting period τ_2, and the detection period τ_3. For a time ordering $t_\gamma \geq t_\beta \geq t_\alpha$ ($\{\alpha, \beta, \gamma\} = \{a, b, c\}$), the three intervals are defined by $\tau_1 \equiv t_\beta - t_\alpha$, $\tau_2 \equiv t_\gamma - t_\beta$, and $\tau_3 \equiv t - t_\gamma$. By varying the ordering of the three input pulses, we can detect the signals corresponding to various Liouville pathways in the $\boldsymbol{k}_S$ direction. In what follows, the response function for an ordering $t_\gamma \geq t_\beta \geq t_\alpha$ is denoted by $R_{\gamma\beta,\alpha}(\tau_3, \tau_2, \tau_1)$. Then, we have[57]

$$R_{cb,a}(\tau_3, \tau_2, \tau_1) = \mathrm{Tr}\left\{\mu(\hat{\boldsymbol{q}})\, \hat{G}(\tau_3) \frac{i}{\hbar}\hat{\mu}_{\rightarrow}^{\times}\, \hat{G}(\tau_2) \frac{i}{\hbar}\hat{\mu}_{\rightarrow}^{\times}\, \hat{G}(\tau_1) \frac{i}{\hbar}\hat{\mu}_{\leftarrow}^{\times} \hat{\rho}_{\mathrm{tot}}^{\mathrm{eq}}\right\} \tag{3.10a}$$

$$R_{ca,b}(\tau_3, \tau_2, \tau_1) = \mathrm{Tr}\left\{\mu(\hat{\boldsymbol{q}})\, \hat{G}(\tau_3) \frac{i}{\hbar}\hat{\mu}_{\rightarrow}^{\times}\, \hat{G}(\tau_2) \frac{i}{\hbar}\hat{\mu}_{\leftarrow}^{\times}\, \hat{G}(\tau_1) \frac{i}{\hbar}\hat{\mu}_{\rightarrow}^{\times} \hat{\rho}_{\mathrm{tot}}^{\mathrm{eq}}\right\} \tag{3.10b}$$

and

$$R_{ac,b}(\tau_3, \tau_2, \tau_1) = \mathrm{Tr}\left\{\mu(\hat{\boldsymbol{q}})\, \hat{G}(\tau_3) \frac{i}{\hbar}\hat{\mu}_{\leftarrow}^{\times}\, \hat{G}(\tau_2) \frac{i}{\hbar}\hat{\mu}_{\rightarrow}^{\times}\, \hat{G}(\tau_1) \frac{i}{\hbar}\hat{\mu}_{\rightarrow}^{\times} \hat{\rho}_{\mathrm{tot}}^{\mathrm{eq}}\right\} \tag{3.10c}$$

where $\hat{G}(\tau)$ is the retarded propagator of the total system in the Liouville space. The operator $\hat{\mu}_{\rightarrow}$ is defined by

$$\hat{\mu}_{\rightarrow} \equiv \sum_{v,v'} |v+1, v'\rangle\langle v+1, v'|\mu(\hat{\boldsymbol{q}})|v, v'\rangle\langle v, v'| \tag{3.11}$$

for the dipole moment of the system $\mu(\boldsymbol{q})$, and the operator $\hat{\mu}_{\leftarrow}$ is the Hermitian conjugate of $\hat{\mu}_{\rightarrow}$. Note that the directions of the subscript arrows in eq 3.10 correspond to those of the arrows in double-sided Feynman diagrams. The response functions, eqs 3.10a and 3.10b, describe the rephasing and nonrephasing experiments, respectively. When $\tau_2 = 0$, however, the last two pulses are coincident in the matter. Then, the two response functions stemming from the different time orderings, $R_{cb,a}$ and $R_{bc,a}$ ($= R_{cb,a}$), are indistinguishable for the rephasing experiment. By the same token, both of the two response functions, $R_{ca,b}$ and $R_{ac,b}$, contribute to the nonrephasing signal when τ_2

$= 0$. Therefore, we redefine the rephasing and nonrephasing response functions as

$$R_R(\tau_3, \tau_2, \tau_1) \equiv H(\tau_2)\, R_{cb,a}(\tau_3, \tau_2, \tau_1) + H(-\tau_2)\, R_{bc,a}(\tau_3, -\tau_2, \tau_1) \quad (3.12)$$

and

$$R_{NR}(\tau_3, \tau_2, \tau_1) \equiv H(\tau_2)\, R_{ca,b}(\tau_3, \tau_2, \tau_1) + H(-\tau_2)\, R_{ac,b}(\tau_3, -\tau_2, \tau_1) \quad (3.13)$$

respectively, where $H(t)$ is the Heaviside step function.

Here, we describe the way to calculate the optical response function, eq 3.10a, from the equation of motion approach.[49,57] At the setout, we have to generate the true equilibrium state of the reduced density matrix. The equilibrium state should include the correlation effect between the system and the bath, which arises from the system−bath interaction. To have the correlated equilibrium state, we temporally set an initial condition, $\hat{\rho}(\boldsymbol{J} = \mathbf{0}, t_i) = \exp(-\beta\hat{H})/\mathrm{Tr}\exp(-\beta\hat{H})$ and $\hat{\rho}(\boldsymbol{J} \neq \mathbf{0}, t_i) = 0$. It should be noted that this temporal initial condition is not the true equilibrium state because it neglects the correlation effect. We can generate the initial equilibrium state by integrating the equation of motion, eqs 2.10 and 2.15, with the temporal condition, until all hierarchical elements attain steady-state values. (See also Appendix A of ref 29.) This time instant is set to be $t = 0$. *If we utilize the theories suffering from the positivity problem mentioned in Section 2, then we cannot obtain the physically meaningful correlated equilibrium state and hence cannot carry forward the calculations anymore. To ignore this fact is to miss the significance of the positivity property.* Next, the generated equilibrium state is modified by the first laser pulse via the dipole operator as $(i/\hbar)\hat{\mu}^{\times}_{-}$. This perturbed density operator is propagated for the τ_1 period by the operator $\hat{G}(\tau_1)$, where the time evolution follows the equation of motion, eqs 2.10 and 2.15. The subsequent events can be interpreted correspondingly. Finally, the expectation value of the dipole moment $\mu(\hat{\boldsymbol{q}})$ is calculated with the density operator perturbed by three laser pulses. Equations 3.10b and 3.10c can be calculated in the same way.

By the double Fourier transform of eqs 3.12 and 3.13 with respect to τ_1 and τ_3, we can obtain a 2D rephasing spectrum

$$S_R(\Omega_3, \Omega_1; \tau_2) = \mathrm{Im}\int_0^\infty d\tau_3 \int_0^\infty d\tau_1 e^{i\Omega_3\tau_3 + i\Omega_1\tau_1} R_R(\tau_3, \tau_2, \tau_1) \quad (3.14)$$

and a 2D nonrephasing spectrum

$$S_{NR}(\Omega_3, \Omega_1; \tau_2) = \mathrm{Im}\int_0^\infty d\tau_3 \int_0^\infty d\tau_1 e^{i\Omega_3\tau_3 + i\Omega_1\tau_1} R_{NR}(\tau_3, \tau_2, \tau_1) \quad (3.15)$$

respectively. The individual 2D rephasing and nonrephasing spectra show distorted line shapes (the so-called *phase-twisted* lines) because the double Fourier transform leads to a combination of absorptive and dispersive features.[34] By adding the 2D rephasing and nonrephasing spectra in equal weights, however, we can cancel out the contribution from the dispersive part to obtain the 2D correlation spectrum with only the absorptive line shape:[60]

$$S_C(\Omega_3, \Omega_1; \tau_2) \equiv S_R(\Omega_3, -\Omega_1; \tau_2) + S_{NR}(\Omega_3, \Omega_1; \tau_2) \quad (3.16)$$

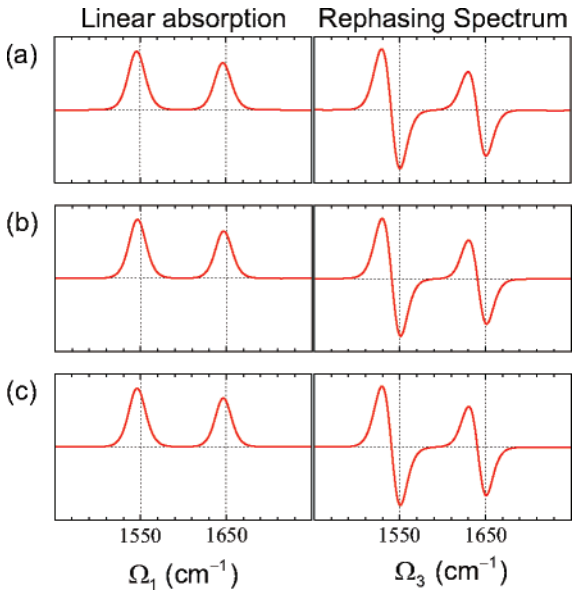

Figure 2. Comparison of the 1D spectra: (a) + correlated fluctuation, (b) − correlated fluctuation, and (c) uncorrelated fluctuation. The left panels show the linear absorption spectra, whereas the right panels the 1D plot of the rephasing spectra, eq 3.17. In the rephasing spectra, the negative-going peaks arise from the 0−1 transition, whereas the positive-going peaks arise from the 1−2 transition.

Figure 2 presents linear absorption spectra (left panels) and 1D plots of the rephasing spectra (right panels) defined by

$$\tilde{S}_R^{(3)}(\Omega_3) = \mathrm{Im}\int_0^\infty d\tau_3 e^{i\Omega_3\tau_3} R_R(\tau_3, \tau_2 = 0, \tau_1 = 0) \quad (3.17)$$

Panels (a), (b), and (c) are for the + correlated, − correlated, and uncorrelated cases, respectively. The 1D spectra for each case have fairly similar characteristics. In the rephasing spectra, the negative-going peaks arise from the 0−1 transition, whereas the positive-going peaks arise from the 1−2 transition. However, one cannot extract any further information from the 1D spectra; it is impossible to distinguish the different mechanisms of the potential surface fluctuation.

The 2D-IR rephasing, nonrephasing, and correlation spectra with $t_2 = 0$ are given in Figure 3. Panels (a) and (b) are for the + correlated and − correlated fluctuation cases, respectively. In spectra (a-iii), the off-diagonal peaks are titled parallel to the diagonal peaks. By comparing the rephasing spectrum (a-i) with the nonrephasing one (a-ii), we can see the peaks arise mainly from the rephasing pathways. In spectra (b-iii), in contrast, the off-diagonal peaks are titled perpendicular to the diagonal peaks. The peaks come mainly from the nonrephasing pathways. The difference between the off-diagonal peak amplitudes in panel (a-i) and those in panel (b-ii) are due to the imbalance contributions among the number of the Liouville pathways for the rephasing and nonrephasing processes. (See Figure 4.) These results are similar to the results by Khalil, Demirdöven, and Tokmakoff.[6] Their analysis was based on a quasi-static energy-level model employing the complete separation of the extremely fast (homogeneous limit: $\Delta_s/\gamma_1 \ll 1$) and extremely slow (inhomogeneous limit: $\Delta_s/\gamma_1 \gg 1$) components for the system−bath interactions. However, we employed a more-general model described by molecular vibrational coordinates and apply the dynamical theory for the spectral diffusion regime with the moderate inhomogeneity, $\Delta_s/\gamma_1 = 1.87$. Thus, the degree of elongation of the 2D lineshapes in Figure 3 along the diagonal axis is less than that in Figure 15 in ref 6. Panel (c) is for the uncorrelated case. In this case, the fluctuations of

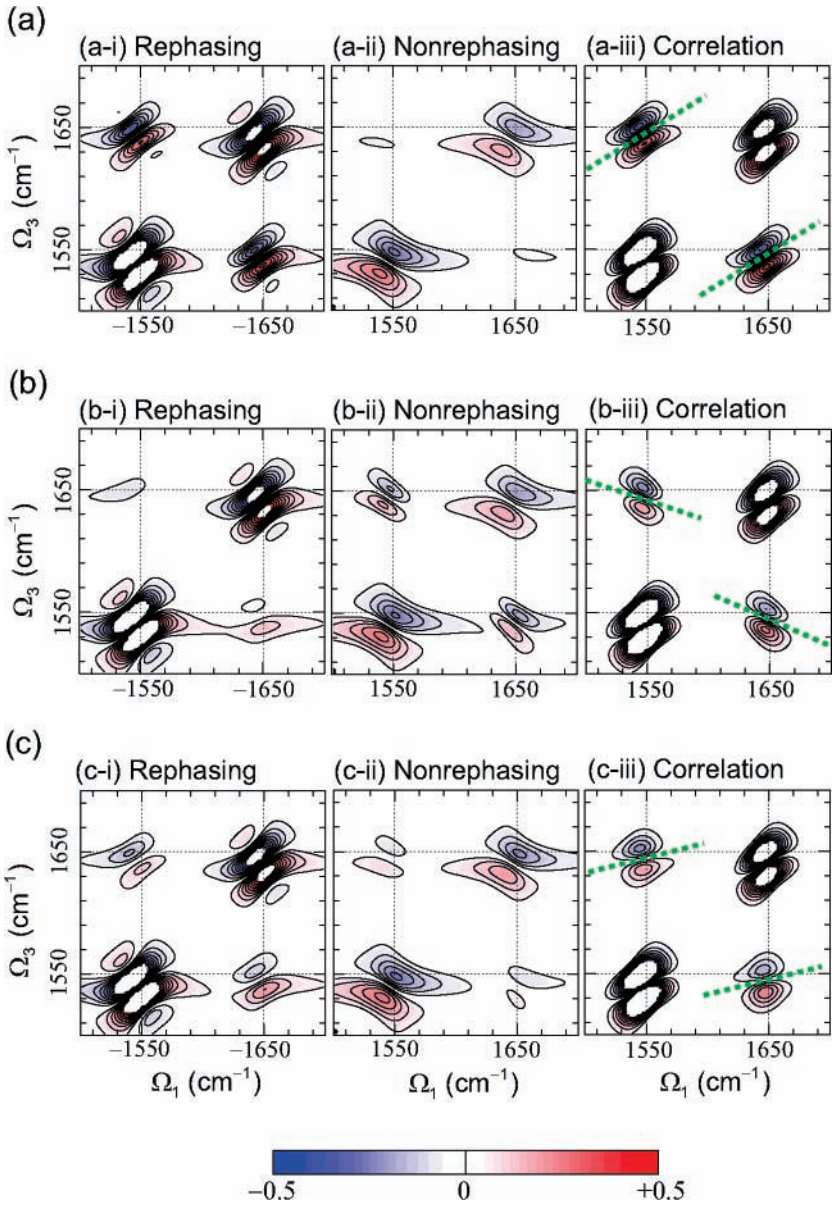

Figure 3. Comparison of 2D-IR spectra: (a) + correlated fluctuation, (b) − correlated fluctuation, and (c) uncorrelated fluctuation. The panels from the left to right show (i) the rephasing spectra, eq 3.14; (ii) the nonrephasing spectra, eq 3.15; and (iii) the correlation spectra, eq 3.16, respectively. The normalization of 2D plots is such that the peak amplitude at $(\Omega_1, \Omega_3) = (1550, 1550)$ cm^{-1} in spectrum a-iii is unity. Twenty equally spaced contour levels from −0.5 to 0.5 are drawn for each plot.

frequencies ω_1 and ω_2 are independent. Therefore, the amplitudes of the off-diagonal peaks in the rephasing spectrum (c-i) is suppressed relative to those in spectrum (a-i) and is enhanced relative to those in (b-i). By the same token, the off-diagonal amplitudes in the nonrephasing spectra (c-ii) are weaker than those in (b-ii) and is stronger than those in (a-i). However, because the number of the Liouville pathways contributing to the spectrum (c-i) is more than that for (c-ii); the gradient of the off-diagonal peaks in the correlation spectrum (c-iii) is slightly upward. Thus, it is difficult to distinguish clearly the difference between the + correlation and the uncorrelation from only the gradients of the off-diagonal peaks in the correlation spectra. We need to analyze the amplitudes of the peaks in the rephasing and nonrephasing spectra.

4. Concluding Remarks

In this paper, we extended the quantum Fokker−Planck equation with low-temperature correction terms to the multimode system coupled to the multiple heat baths. Previous studies on the multimode systems, which utilized the Redfield equation and the stochastic theories, started from the energy-level representation. In contrast, our formalism is based on a molecular coordinate representation although we used energy eigenstates to carry out numerical calculations. By means of the present formalism, 1D- and 2D-IR spectra for the two-mode systems were calculated for various conditions. We showed that, in contrast to the 1D spectra, the 2D spectra were very sensitive to the distinct manners of the potential surface modulation. We discussed correlation effects of modulation between the two modes. For this purpose, we consider two cases of system−bath couplings. One is a correlated case in which two modes are coupled to a single bath, and the other is an uncorrelated case in which each mode is coupled to a respective baths. We further classify the correlated case into two cases, the +correlation and − correlation cases. In the + correlation case, the bath modulates the curvatures of the two modes in the same direction. Alternatively, in the − correlation case, the bath modulates the curvatures in opposite directions. No information

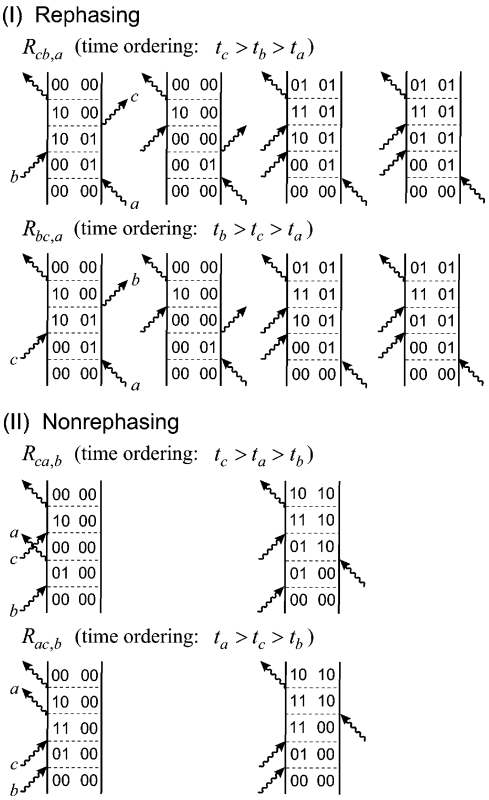

Figure 4. Double-sided Feynman diagrams representing the Liouville pathways, which cause the off-diagonal peaks in the lower right of the rephasing spectra and the nonrephasing spectra in Figure 3. A set of four numbers horizontally arranged in a diagram, $|v_1v_2\ v_1'v_2'|$ means the coherence between $|v_1\rangle \otimes |v_2\rangle = |v_1v_2\rangle$ and $|v_1'\rangle \otimes |v_2'\rangle = |v_1'v_2'\rangle$, i.e., $|v_1v_2\rangle\langle v_1'v_2'|$. One can obtain the diagrams for the off-diagonal peaks in the upper left by interchanging 01 and 10. Note that there are twice as many rephasing pathways as nonrephasing ones.

on the correlated and uncorrelated effects could not be extracted from the 1D spectra. However, the difference between the distinct correlation and uncorrelation manners were clearly observed by the 2D spectra.

In this paper, we discussed the effects of the bath modulation mainly on the vibrational phase relaxation processes. However, our approach can also be applied to the vibrational energy transfer processes. As is well known, the intramolecular vibrational energy redistribution processes are closely related to the thermal chemical reaction processes. Monitoring the reaction processes on multidimensional potential surfaces by means of the 2D-IR spectroscopy is interesting and challenging. In addition, our formalism is not limited to the vibrational motions. By considering two-level systems instead of anharmonic oscillators, we can deal with a variety of systems such as coupled multichromophore systems. For those systems, 2D electronic spectra provide detailed information on the electronic couplings among chromophores and on the excited energy and coherence transfer.[61−65] We leave them for future studies.

Acknowledgment. A.I. appreciates the support of Research Fellowships of the Japan Society for the Promotion of Science for Young Scientists, no.18-2691. Y.T. is grateful for the financial support from Grant-in-Aid for Scientific Research A 15205005 and for Priority Area of "Molecular Theory for Real Systems'' (18066018) from the Japan Society for the Promotion of Science.

References and Notes

(1) Tanimura, Y.; Mukamel, S. *J. Chem. Phys.* **1993**, *99*, 9496.
(2) Mukamel, S.; Piryatinski, A.; Chernyak, V. *Acc. Chem. Res.* **1999**, *32*, 145.
(3) Mukamel, S. *Annu. Rev. Phys. Chem.* **2000**, *51*, 691.
(4) Woutersen, S.; Hamm, P. *J. Phys.: Condens. Matter* **2002**, *14*, R1035.
(5) Jonas, D. M. *Annu. Rev. Phys. Chem.* **2003**, *54*, 425.
(6) Khalil, M.; Demirdoven, N.; Tokmakoff, A. *J. Phys. Chem. A* **2003**, *107*, 5258.
(7) Hochstrasser, R. M. *Adv. Chem. Phys.* **2006**, *132*, 1.
(8) Cho, M. *Bull. Korean Chem. Soc.* **2006**, *27*, 1940.
(9) Hamm, P.; Lim, M.; Hochstrasser, R. M. *J. Phys. Chem. B* **1998**, *102*, 6123.
(10) Woutersen, S.; Hamm, P. *J. Phys. Chem. B* **2000**, *104*, 11316.
(11) Asplund, M. C.; Zanni, M. T.; Hochstrasser, R. M. *Proc. Natl. Acad. Sci. U.S.A.* **2000**, *97*, 8219.
(12) Zanni, M. T.; Gnanakaran, S.; Stenger, J.; Hochstrasser, R. M. *J. Phys. Chem. B* **2001**, *105*, 6520.
(13) Maekawa, H.; Toniolo, C.; Moretto, A.; Broxterman, Q. B.; Ge, N. H. *J. Phys. Chem. B* **2006**, *110*, 5834.
(14) Torii, H. *J. Phys. Chem. A* **2006**, *110*, 4822.
(15) Fujisaki, H.; Straub, J. E. *J. Phys. Chem. B* **2007**, in press.
(16) Merchant, K. A.; Noid, W. G.; Akiyama, R.; Finkelstein, I. J.; Goun, A.; McClain, B. L.; Loring, R. F.; Fayer, M. D. *J. Am. Chem. Soc.* **2003**, *125*, 13804.
(17) Chung, H. S.; Khalil, M.; Tokmakoff, A. *J. Phys. Chem. B* **2004**, *108*, 15332.
(18) Demirdoven, N.; Cheatum, C. M.; Chung, H. S.; Khalil, M.; Knoester, J.; Tokmakoff, A. *J. Am. Chem. Soc.* **2004**, *126*, 7981.
(19) Asbury, J. B.; Steinel, T.; Stromberg, C.; Corcelli, S. A.; Lawrence, C. P.; Skinner, J. L.; Fayer, M. D. *J. Phys. Chem. A* **2004**, *108*, 1107.
(20) Woutersen, S.; Mu, Y.; Stock, G.; Hamm, P. *Chem. Phys.* **2001**, *266*, 137.
(21) Asbury, J. B.; Steinel, T.; Stromberg, C.; Gaffney, K. J.; Piletic, I. R.; Goun, A.; Fayer, M. D. *Phys. Rev. Lett.* **2003**, *91*, 237402.
(22) Kwac, K.; Lee, H.; Cho, M. *J. Chem. Phys.* **2004**, *120*, 1477.
(23) Rubtsov, I. V.; Kumar, K.; Hochstrasser, R. M. *Chem. Phys. Lett.* **2005**, *402*, 439.
(24) Cowan, M. L.; Bruner, B. D.; Huse, N.; Dwyer, J. R.; Chugh, B.; Nibbering, E. T. J.; Elsaesser, T.; Miller, R. J. D. *Nature* (*London*) **2005**, *434*, 199.
(25) Kolano, C.; Helbing, J.; Kozinski, M.; Sander, W.; Hamm, P. *Nature* (*London*) **2006**, *444*, 469.
(26) Ohta, K.; Maekawa, H.; Saito, S.; Tominaga, K. *J. Phys. Chem. A* **2003**, *107*, 5643.
(27) Ohta, K.; Tominaga, K. *Bull. Chem. Soc. Jpn.* **2005**, *78*, 1581.
(28) Kühn, O.; Tanimura, Y. *J. Chem. Phys.* **2003**, *119*, 2155.
(29) Ishizaki, A.; Tanimura, Y. *J. Chem. Phys.* **2005**, *123*, 014503.
(30) Giese, K.; Petkovic, M.; Naundorf, H.; Kühn, O. *Phys. Rep.* **2006**, *430*, 211.
(31) Zheng, J.; Kwak, K.; Asbury, J.; Chen, X.; Piletic, I. R.; Fayer, M. D. *Science* **2005**, *309*, 1338.
(32) Kim, Y. S.; Hochstrasser, R. M. *Proc. Natl. Acad. Sci. U.S.A.* **2005**, *102*, 11185.
(33) Sanda, F.; Mukamel, S. *J. Chem. Phys.* **2006**, *125*, 014507.
(34) Ernst, R. R.; Bodenhausen, G.; Wokaun, A. *Principles of Nuclear Magnetic Resonance in One and Two Dimensions*; Oxford University Press: New York, 1990.
(35) Cho, M. H.; Okumura, K.; Tanimura, Y. *J. Chem. Phys.* **1998**, *108*, 1326.
(36) Okumura, K.; Tokmakoff, A.; Tanimura, Y. *J. Chem. Phys.* **1999**, *111*, 492.
(37) Okumura, K.; Jonas, D. M.; Tanimura, Y. *Chem. Phys.* **2001**, *266*, 237.
(38) Kim, H.-D.; Tanimura, Y. *J. Chem. Phys.* **2005**, *123*, 224310.
(39) Hahn, S.; Kim, S.-S.; Lee, C.; Cho, M. *J. Chem. Phys.* **2005**, *123*, 084905.
(40) Goj, A.; Loring, R. F. *J. Chem. Phys.* **2006**, *124*, 194101.
(41) Okumura, K.; Tokmakoff, A.; Tanimura, Y. *Chem. Phys. Lett.* **1999**, *314*, 488.
(42) Redfield, A. G. *Adv. Magn. Reson.* **1965**, *1*, 1.
(43) Ishizaki, A.; Tanimura, Y. *Chem. Phys.*, submitted, 2007.
(44) Tanimura, Y.; Kubo, R. *J. Phys. Soc. Jpn.* **1989**, *58*, 101.
(45) Tanimura, Y.; Wolynes, P. G. *Phys. Rev. A* **1991**, *43*, 4131.
(46) Tanimura, Y.; Steffen, T. *J. Phys. Soc. Jpn.* **2000**, *69*, 4095.
(47) Kato, T.; Tanimura, Y. *J. Chem. Phys.* **2002**, *117*, 6221.
(48) Kato, T.; Tanimura, Y. *J. Chem. Phys.* **2004**, *120*, 260.
(49) Tanimura, Y. *J. Phys. Soc. Jpn.* **2006**, *75*, 082001.
(50) Schröder, M.; Schreiber, M.; Kleinekathöfer, U. *J. Chem. Phys.* **2007**, *126*, 114102.
(51) Tanimura, Y. *Phys. Rev. A* **1990**, *41*, 6676.
(52) Ishizaki, A.; Tanimura, Y. *J. Phys. Soc. Jpn.* **2005**, *74*, 3131.
(53) Shao, J. *J. Chem. Phys.* **2004**, *120*, 5053.

(54) Xu, R. X.; Cui, P.; Li, X. Q.; Mo, Y.; Yan, Y. J. *J. Chem. Phys.* **2005**, *122*.

(55) Xu, R.-X.; Yan, Y. *Phys. Rev. E* **2007**, *75*, 031107.

(56) Jin, J. S.; Welack, S.; Luo, J. Y.; Li, X. Q.; Cui, P.; Xu, R. X.; Yan, Y. J. *J. Chem. Phys.* **2007**, *126*.

(57) Ishizaki, A.; Tanimura, Y. *J. Chem. Phys.* **2006**, *125*, 084501.

(58) Demirdoven, N.; Khalil, M.; Tokmakoff, A. *Phys. Rev. Lett.* **2002**, *89*, 237401.

(59) Feynman, R. P.; Vernon, F. L. *Ann. Phys.* (*N.Y.*) **1963**, *24*, 118.

(60) Khalil, M.; Demirdoven, N.; Tokmakoff, A. *Phys. Rev. Lett.* **2003**, *90*, 047401.

(61) Brixner, T.; Stenger, J.; Vaswani, H. M.; Cho, M.; Blankenship, R. E.; Fleming, G. R. *Nature* **2005**, *434*, 625.

(62) Cho, M.; Vaswani, H. M.; Brixner, T.; Stenger, J.; Fleming, G. R. *J. Phys. Chem. B* **2005**, *109*, 10542.

(63) Engel, G. S.; Calhoun, T. R.; Read, E. L.; Ahn, T.-K.; Mancal, T.; Cheng, Y.-C.; Blankenship, R. E.; Fleming, G. R. *Nature* **2007**, *446*, 782.

(64) Lee, H.; Cheng, Y.-C.; Fleming, G. R. *Science* **2007**, *316*, 1462.

(65) Kim, H.-D.; Tanimura, Y.; Cho, M. *J. Chem. Phys.* **2007**, *127*, 075101.